Confirmation of Sub-Cellular Resolution Using Oversampling Imaging Mass Spectrometry

Albert Maimó-Barceló[1], Jone Garate[2], Joan Bestard-Escalas[1], Roberto Fernández[2,a], Luzie Berthold[1,3], Daniel H. Lopez[1], José A. Fernández[2,*] and Gwendolyn Barceló-Coblijn[1,*]

[†] Lipids in Human Pathology, Institut d'Investigació Sanitària Illes Balears (IdISBa) – Health Research Institute of the Balearic Islands, Ctra. Valldemossa 79, Module I, Floor -1, E-07120, Palma, Balearic Islands, Spain

[‡] Department of Physical Chemistry, Fac. of Science and Technology, University of the Basque Country (UPV/EHU), Barrio Sarriena s/n, 48940 Leioa, Spain

[×] Bioanalytical Department, Technical University of Berlin, Straße des 17. Juni 135, 10623 Berlin, Germany

KEYWORDS. MALDI-imaging • lateral resolution • oversampling • colonocytes • nucleus

[a]Present address: Department of Research and Development, IMG Pharma Biotech S.L., Derio 48160, Spain.

Correspondence to:

José Andrés Fernández, Ph.D., Department of Physical Chemistry, Fac. of Science and Technology, University of the Basque Country (UPV/EHU), Barrio Sarriena s/n, 48940 Leioa, Spain, email: josea.fernandez@ehu.es;

Gwendolyn Barceló-Coblijn, Ph.D., Institut d'Investigació Sanitària Illes Balears (IdISBa, Health Research Institute of the Balearic Islands), Carretera de Valldemossa 79, E-07120 Palma, Balearic Islands, Spain, gwendolyn.barcelo@ssib.es ;

Abstract

The use of oversampling in MALDI (matrix-assisted laser desorption/ionization) imaging mass spectrometry (IMS) to improve lateral resolution is a common practice. However, its application is still controversial and recent studies reported a spot size-dependent change in the relative intensity of the spectra. Previously, using oversampling, we described the lipidome of the human colon epithelium, a 20-30 μm width cell monolayer; even assessing the changes occurring within this monolayer associated with complex biological processes. Interestingly, the k-means analysis of those experiments unveiled the presence of a third epithelial cluster that anatomically matched the nuclei position. Taking into account the nucleus size (9-12 μm of diameter) and its distinctive lipidome, we decided to test whether this cluster was really of nuclear origin. Hence, the spectra obtained directly from tissue sections were compared with those recorded from the nuclei isolated from colon biopsies. The highest correlation coefficient was obtained when comparing the spectrum of the isolated nuclei with that of the tissue nuclear cluster, demonstrating the successful identification of the nuclear lipidome in the MALDI-IMS experiments run using oversampling and a lateral resolution of 10 μm/pixel. Importantly, it was established that phosphatidylinositol 38:4 nuclear levels remained stable along the colon crypt. That is, it mimicked neither the regular decrease observed in the epithelium nor the regular increase observed in the stroma, eliminating the chance of inter-pixel contamination. Altogether, besides confirming the usefulness of the oversampling technique, these results strongly reinforce the pivotal role IMS may have in promising fields such as single-cell analysis.

Introduction

In its short lifetime, imaging mass spectrometry (IMS) has proven not only to be a powerful technique to identify changes in cell and tissue homeostasis in the context of a disease, but also to investigate the role lipids and proteins play in a given tissue, or even within each of the different cell types comprising it [1–3]. Among the several desorption techniques used for IMS, MALDI (matrix-assisted laser desorption/ionization) offers a good compromise between sensitivity and lateral resolution [4]. Yet it is a technique prone to experimental pitfalls and data misinterpretation. Despite significant advances in the field, several aspects of the technique are still open questions, such as signal normalization or statistical analysis [5]. In this context, the real lateral resolution of a given MALDI image, particularly when using oversampling, remains a controversial issue.

Introduced by Sweedler's group, the oversampling method uses overlapping laser shots to improve the lateral resolution of IMS images beyond the laser spot size [6]. In this way, images with a pixel size several times smaller than the spot size have been reported [7–14]. However, some studies raise certain concerns regarding the technique, arguing that it may alter the results regarding composition [12, 15–17]. In this line, Dreisewerd's group reported spot size-dependent changes in the relative intensity of the spectra obtained from the white and gray matter of mouse brain sections, using oversampling IMS [17]. Furthermore, although pixel size was maintained constant, the true lateral resolution achieved in these experiments declined as the laser spot increased. Hence, such results introduced doubts concerning the IMS results obtained using oversampling. Taking into account the fact that oversampling is a technique routinely used worldwide in many research laboratories to assess the distribution of proteins and metabolites with a higher level of detail, this issue is a matter of considerable concern. As we and others have demonstrated [7–10, 18–20], a minimum spatial resolution is necessary to enable tissue imaging at the cellular level to correlate the observed changes in composition with the subjacent metabolic mechanism [21]. Furthermore, many studies could be introducing (a mild) oversampling inadvertently by using high laser fluences, which increases the laser spot size.

Materials and methods

Materials and reagents. 1,5-diaminonaphtalene (DAN) matrices, as well as hematoxylin and eosin for histological staining, were purchased from Sigma–Aldrich Chemie (Steinheim, Germany). Water, methanol, acetonitrile, 2-propanol, and formic acid (Fisher Scientific, Fair Lawn, NJ, USA) were obtained from Optima® LC/MS grade. Leucine Enkephalin acetate hydrate, ammonium acetate, and sodium hydroxide solution were purchased from Sigma–Aldrich Chemie.

Human sample collection. Sample collection for this study was specifically approved by the Ethics Research Committee of the Balearic Islands (IB 2118/13 PI). Informed consent was obtained in writing from each patient before performing each endoscopy. Human colon biopsies were obtained in the Endoscopic Room of Hospital Universitari Son Espases (Palma, Spain). Endoscopic biopsies were resected using a Radial Jaw Standard Capacity Biopsy Forceps (Radial Jaw™ 4, Boston Scientific, USA) and immediately snap frozen in liquid nitrogen and saved at −80°C until sample preparation. Sections of ~10 µm thickness were prepared — using no cryoprotective substances or embedding material in a cryostat (Leica CM3050S, Wetzlar, Germany) — at −20°C and placed on plain glass microscope slides. A consecutive section was stained with hematoxylin and eosin for structure identification.

Nuclei isolation. Nuclei were isolated from three human colonoscopic biopsies from three different patients by differential centrifugation. Briefly, biopsies were washed with standard phosphate buffer saline (PBS) and cut into 1-2 cm fragments using scissors. Colon tissue was digested using 10 mM DTT for 5 min and then with 8 mM EDTA (in PBS) for 30 min to separate the epithelium layer from the lamina propria. To help separation, the suspension was vigorously shaken. The supernatant was collected and centrifuged at 100 ×g for 10 min at 4°C. The pellet of crypts was resuspended in 500 µl of PBS and sonicated (2 sec at 10% amplitude), and further centrifuged at 100 ×g for 5 min at 4°C. The supernatant was centrifuged at 1500 ×g for 5 min at 4°C, and the remaining nuclei enriched pellet was stored at -80°C. To assess the quality of the fraction in terms of purity, an aliquot of the nuclei enriched fraction was resuspended in PBS and stained with hematoxylin and eosin using standard protocols. A second aliquot of a confirmed highly enriched fraction was stained with DAPI (specific for nuclei) following the protocol described in Bestard et al [8, 9]. Finally, a third aliquot was resuspended in methanol for posterior MALDI-MS analysis.

MALDI-IMS analysis. Four histological sections obtained from three different patients were prepared and analyzed by MALDI-IMS as described in Garate et al [7]. Briefly, DAN (1,5-diaminonaphtalene) was used as matrix for negative-ion detection, deposited with the aid of a glass sublimator (Ace Glass 8023). Four sections of colonoscopic biopsies from different individuals were scanned in negative-ion mode, using the orbitrap analyzer of a MALDI-LTQ-Orbitrap XL (Thermo Fisher, San Jose, CA, USA). The MALDI source used in this study was the one provided by the manufacturer, which is equipped with a N_2 laser (LTB, Berlin, model MNL 100, 100 µJ max power, elliptical spot, 60 Hz repetition rate), and a very simple optical arrangement, consisting of two mirrors and a single focusing lens of f = 125 mm. Laser energy for IMS and nuclei isolated fractions was 30-60 µJ, and 80 µJ respectively. Laser spot dimension was elliptical as previously described in Garate et al [7]. The step-size used for oversampling was 10 µm, with complete sample ablation (20 laser shots per spot or pixel). Mass resolutions of 30,000 and 100,000 at m/z = 400 Da were used to record tissue sections and isolated nuclei data, respectively, and the scanning range was 550–1200 Da in negative-ion mode. Lipid assignment was based on the comparison between the experimental m/z and the species in the software's database (<33,000 lipid species plus adducts) and in the lipid maps database (www.lipidmaps.org). Mass accuracy was always better than 9 ppm and was typically better than 3 ppm. In this type of analyzers, mass

accuracy depends somehow on the intensity of the peaks, and thus, the m/z with higher intensity present better mass accuracy. In the cases where no univocal assignment was found, a comparison with the data from UHPLC–MS/MS was performed. Detailed information UHPLC–MS/MS and MS/MS may be found in Fernandez et al [22] and in the Suppl. Material of Bestard-Escalas et al [9]. If any of the candidates was not detected by UHPLC–MS, and was not detected as another adduct in the MALDI-IMS experiment, this candidate was not considered for assignment. The spectra were analyzed using dedicated software (MSIAnalyst2.0; NorayBioinformatics S.L., Bilbao, Spain). For more details see supplementary information on previous publications [7–9].

Statistical analysis: To establish the tissue clusters, non-supervised K-means analysis (MSI-Analyst 2.0, NorayBio) was used, setting the number of segments (k) to 6-8, including the tissue nuclear cluster. The results include four independent measurements on four different tissue sections obtained from three patients. Correlation coefficients between spectrum of nuclear fraction and the spectrum associated to each of the segments established by k-means were calculated using Microsoft® Excel. Version 16.20.

Results and discussion

The recent reports on intensity modulation due to oversampling prompted us to run a set of experiments to validate the results previously obtained in human colon sections. Thus, we report that using oversampling IMS at a pixel size of 10 µm, it is possible to evaluate the lipidomic changes that take place exclusively in the colon epithelium, associated with the tumorigenic process [7–9]. Beyond their undeniable biological implications, these results are particularly relevant because the colon epithelium consists of a 20-30 µm width single-cell monolayer, indicating therefore that we had indeed reached cellular resolution. Further, this monolayer invaginates into the lamina propria (stromal tissue) generating a cylindrical structure called crypt, wherein at the bottommost reside the adult stem cells that divide and differentiate into fully mature colonocytes while ascending towards the lumen. Using MALDI-IMS in oversampling mode at this pixel size, we were also able to follow the changes occurring within the monolayer, from the bottom to the top of the crypt [7–9]. These results reveal a stunning regulation of the lipidome, which appears to be intimately associated with the differentiation process. Thus, as colonocyte maturation proceeds, membrane lipids containing monounsaturated fatty acids increase according to a first-degree equation ($y=ax+b$, R^2=0.95-0.98, green colonocytes in Fig. 4), while those containing arachidonic acid decrease according to a logarithmic equation ($y=-\ln(x)+b$, R^2=0.95-0.98, pink colonocytes in Fig. 4) [8, 9]. This specificity translates into the formation of two lipid clusters (generated by the k-means analysis) within the epithelium monolayer, dividing the colon crypt into two halves: the upper cluster and the lower cluster containing the most differentiated and least differentiated, respectively. However, we also obtained a third cluster consisting, mostly, of a non-continuous thin line running longitudinally through the crypt (Fig. 1). A close comparison with the consecutive HE-stained section indicated that this cluster was not in the stroma but in the epithelium, and did coincide with the position of the nuclei. Importantly, in colon epithelium, the small, round-shaped nuclei (9-12 µm of diameter) are always located basally. Both nuclear shape and location are strictly regulated, and any variation in these parameters is a sign of alert pointing to a dysplastic transformation for pathologists. Finally, it is well established that the nucleus has a distinct lipidome and lipid metabolism [23–25]. Therefore, it would be consistent with the lipid fingerprint of these pixels being sufficiently different from those of the rest of the image to generate a new cluster.

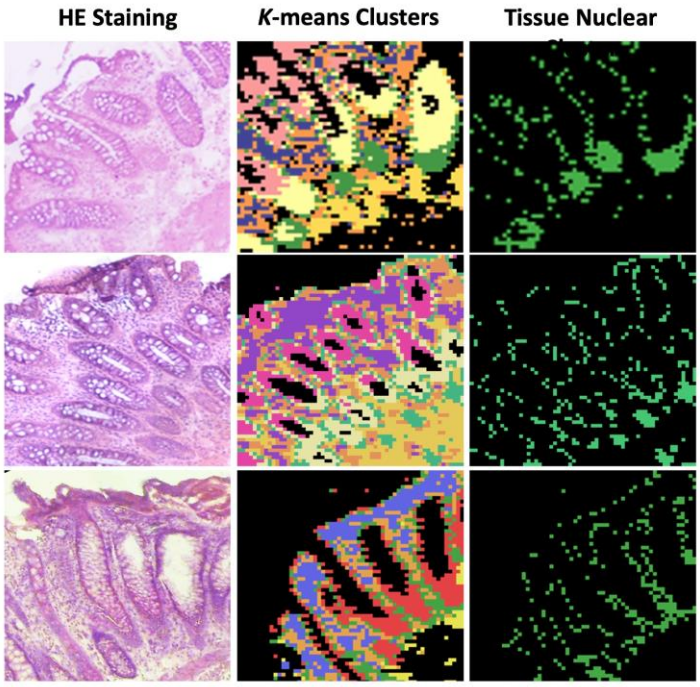

Fig. 1 Cluster analysis by the k-means of MALDI-IMS experiments. Representative results obtained from healthy colon mucosa led consistently to the formation of a third epithelial cluster – identified as "Tissue Nuclear Cluster" (right column) – that fits anatomically with the characteristic polarized position of the nuclei in colonocytes (left column). All experiments were recorded using oversampling, at 10 μm/pixel of lateral resolution, and in negative-ion mode (more details may be found in Garate et al [7]). Scale bar = 50 μm. Four histological sections obtained from three different patients were analyzed. the tissue clusters established using non-supervised K-means analysis (MSI-Analyst 2.0, NorayBio), setting the number of segments (k) to 6-8.

All these arguments strongly indicate that the formation of the third epithelial cluster was due, on the one hand, to the presence of cell nuclei, and on the other hand, to the specific detection of nuclear lipids, and that, consequently, we were able to establish the lipidome of a subcellular organelle. To test this hypothesis, human colonocyte nuclei were isolated from biopsies using standard differential centrifugation methods, and analyzed by MALDI. The purity of the nuclear fraction was verified by flow cytometry, using DAPI as a marker for nuclei (data not shown). The isolated fraction was placed on a standard MALDI plate and covered with the matrix to record their lipid fingerprint by MALDI as was done for the tissue sections (Fig. 2A). This spectrum (Fig. 2A) was then compared with the average spectra of each of the clusters obtained during the IMS experiments on tissue sections. A simple visual inspection of the spectra shows that the lipid fingerprint of the isolated nuclei (Fig. 2A) offers the best match with that of the tissue nuclear cluster (Fig. 2B).

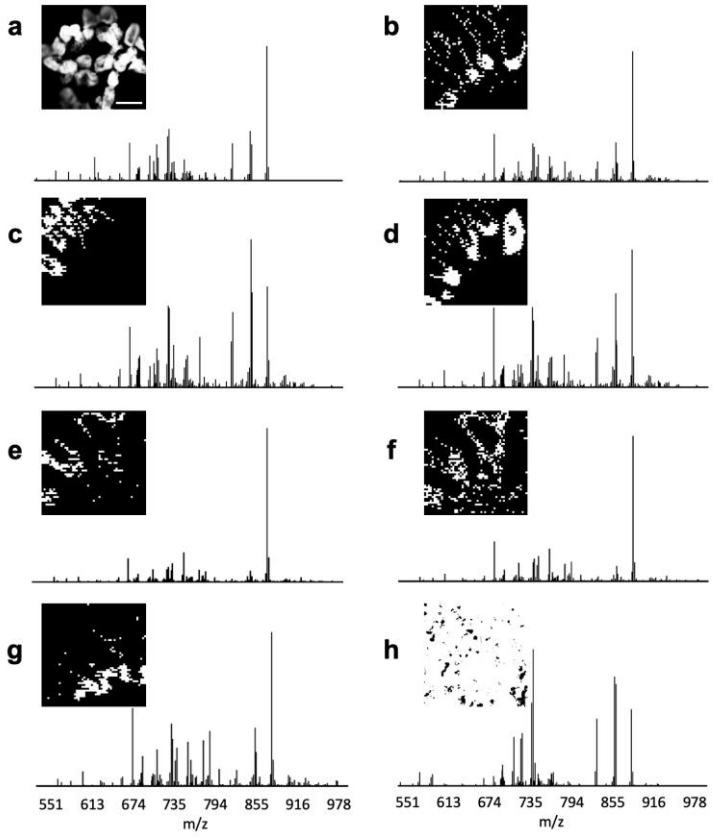

Fig. 2 Average spectra of the MALDI-IMS analysis. a Spectrum of the isolated nuclear fraction. Scale bar = 10 μm. **b-g** Average spectra of clusters obtained after analysis of human colonoscopic sections by MALDI-IMS. **b** Putative tissue nuclear cluster. **c** Cluster including the most-differentiated colonocytes. **d** Cluster including the least-differentiated colonocytes. **e-g** Clusters established in the colon stromal tissue. **h** Spectra of the poorly-enriched nuclear fraction. Insets in **a** and **h** show the microscope images of an aliquot of the sample obtained by differential centrifugation stained with DAPI (specific nuclear dye) or hematoxylin, respectively. **b-g** Clusters associated with each spectrum. All experiments were recorded in negative-ion mode using oversampling and at 10 μm/pixel of lateral resolution (more details may be found in Garate et al. [7]).

To quantitatively support this observation, the correlation coefficient between the spectrum of the isolated nuclei and the spectra of the tissue clusters was calculated (Fig. 3). Consistent with the hypothesis, the correlation to the tissue nuclei cluster obtained the highest value (Figs. 2A vs. 2B, 0.85). Furthermore, the rest of the correlations did not follow an "anatomical proximity" criterion. That is, the clusters near the nuclei did not necessarily exhibit a higher correlation with the spectrum of the isolated nuclei, which could have been an indication of inter-pixel contamination. Interestingly, the lowest correlation was found between the isolated nuclear fraction and the spectrum of a poorly isolated nuclear fraction that contained traces of other cell components (Fig. 2H).

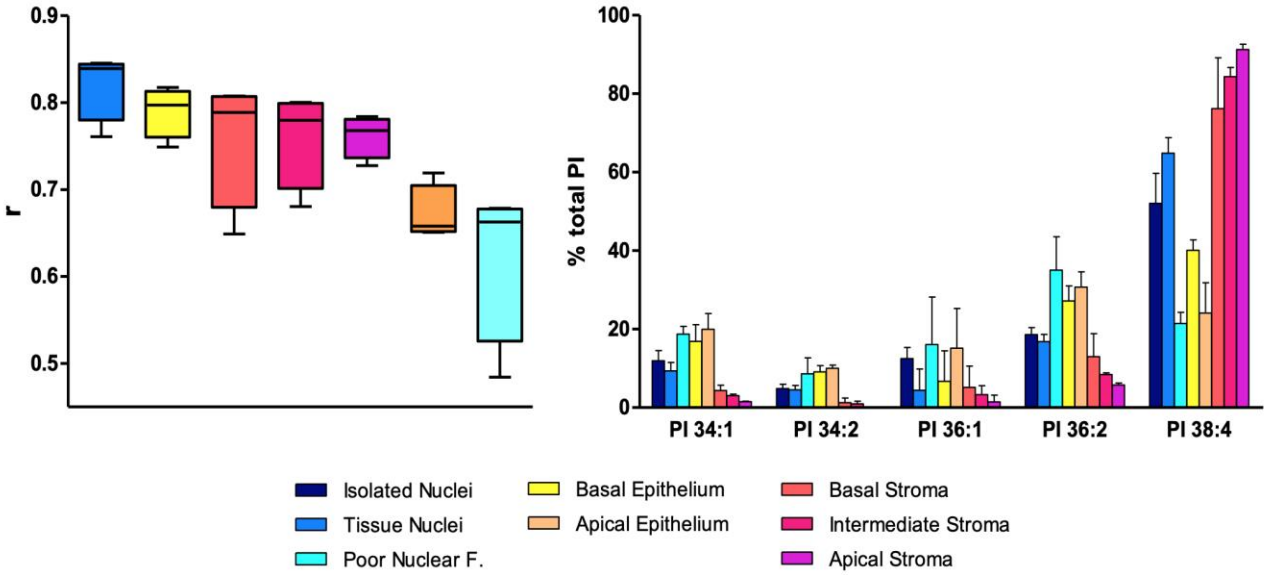

Fig. 3. Comparison between the spectrum of isolated nuclei fractions and the average spectra from tissue clusters. a Correlation coefficient values between average spectra of each of the six tissue clusters established by MALDI-IMS (n=4) and the spectrum of the nuclear fraction (n=3). The figure is a boxplot with the box stretching from the 1st quartile to the 3rd quartile and containing the median in between. The whiskers indicate the minimum and maximum observed value. **b** PI molecular species composition expressed as a percentage of total PI. The values represent the mean ± SD (n = 3), n = biological replicates.

To delve into the differences and similarities between the clusters, their composition was compared in terms of lipid categories. Phosphatidylinositol (PI) species dominated the mass spectrum in negative-ion mode, accounting for most of the signal intensity. Fig. 3B shows the PI molecular species composition of the isolated nuclear fraction, the fraction poorly enriched in nuclei, and the tissue clusters established using non-supervised K-means analysis (MSI-Analyst 2.0, NorayBio), setting the number of segments (k) to 6-8, including the tissue nuclear cluster. Consistent with the correlation data, the most similar PI species distribution to that of the isolated nuclei was the tissue nuclear cluster. Next, taking into account the strict regulation of the epithelial PI species described in our previous studies [8, 9], we investigated whether similar changes would be occurring in nuclei as colonocytes differentiated. Fig. 4A shows an expanded view of one of the crypts included in Fig. 1, wherein a path was outlined in the tissue nuclear cluster using white pixels, from least (pixel 1) to fully differentiated (pixel 28) colonocytes. Similar to the epithelial and stromal lipidome [8, 9], the changes in the nuclear lipidome were assessed along this path. Unexpectedly, colonocyte differentiation did not impact on PI 38:4 levels, the most affected species in the epithelium. Conversely, in the tissue nuclear cluster, PI 38:4 levels – the most abundant species – remained unaltered regardless of the differentiation state of the colonocyte (Fig. 4B). Importantly, this observation is not only in sharp contrast with the highly regulated decrease described in the epithelium but also with the steady increase observed along the lamina propria (Fig. 4C). It is worth noting that PI 38:4 levels in stromal cells were substantially larger (4-5-fold) than in the epithelium (Fig. 2E-F vs. 2C-D and [9]); therefore, the stable values for PI 38:4 observed along the nuclear path cannot be due to a compensation effect (an experimental artifact) between the changes in the colonocytes and those in the surrounding stromal cells.

Collectively, the anatomical comparison, analytical results, and biological considerations are clearly in the line of confirming the hypothesis that the presence of cell nuclei accounts for the formation of the third cluster identified within the

epithelium monolayer during the analysis of the colon sections. As such, these results support the use of oversampling methods to increase the lateral resolution beyond the subcellular level; and, while doing so, the pixel lipid fingerprint appears not to be substantially modified. It is worth stressing that, to the best of our knowledge, even with the most advanced techniques currently used to isolate cell organelles or colonocytes according to their differentiation state, it would be rather difficult to follow the lipidome changes in the nuclei as was done in this study.

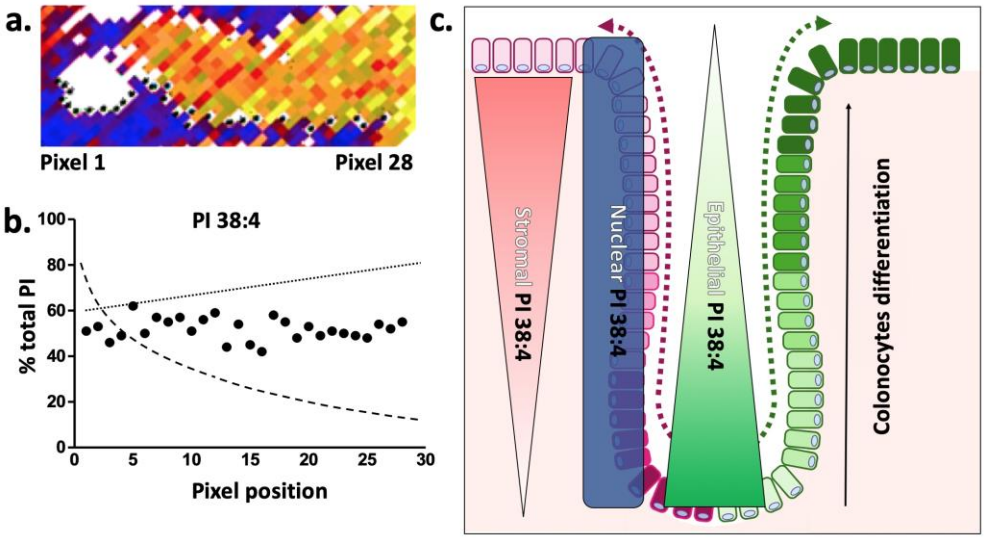

Fig 4 Nuclei PI composition remains unaltered during the colonocyte differentiation process. a Path depicted in the tissue nuclear cluster (in white) to assess the changes occurring in colonocyte nuclei during the differentiation process; **b** PI 38:4 levels, expressed as a percentage of total PI, along the tissue nuclear cluster. The constant values differed from those observed along the epithelium (dashed line) or the stroma (dotted line); **c** Diagram of a colon crypt, consisting of a single cell layer of epithelial cells (colonocytes) that invaginates into the stroma. Adult stem cells (in blue) divide and migrate upwards toward the lumen; during this migration, cells undergo a differentiation process to mature colonocytes. The absence of changes in PI 38:4 levels clearly differed from that observed along the epithelium and the stroma, which decreased and increased from base to lumen, respectively [9].

Conclusions

The results reported herein have important consequences at three levels: analytical, bioanalytical, and biological. At the analytical level, this study reinforces the notion that in order to increase lateral resolution, oversampling is a trustworthy method [6, 7]. At the bioanalytical level, we demonstrate that owing to the oversampling MALDI-IMS methodology, it was possible to establish the lipidome of the cell nuclei, having reached, therefore, the sub-cellular resolution level. Finally, at the biological level, in addition to confirming that the nuclear lipidome is different at the composition level, we were able to reveal that it appears to be regulated differently than the lipidome of the rest of the cell. According to our results, the underlying regulatory mechanisms would be independent of the maturation state of the colonocyte. Nonetheless, there is no doubt that the lateral resolution achieved was a prerequisite in identifying this subcellular organelle.

Studies such as the one reported herein demonstrate that the MALDI-IMS is far from having achieved its full development. In its short lifetime, the technique has generated a remarkable amount of information that, in the near future, will be worth analyzing thoroughly in order to grasp all the knowledge enclosed therein. Taking into account the fact that interest

in describing the whole-cell composition at the single-cell level is increasing exponentially worldwide, our results reinforce the pivotal role that IMS techniques can play in all these initiatives [26].

Compliance with ethical standards

Conflict of interest. The authors declare no competing financial interest.

Acknowledgments. We are greatly thankful to the nurses and the medical doctors of the Gastroenterology Unit of Hospital Universitari de Son Espases (HUSE, Palma, Spain). The Institute of Health Carlos III (CP12/03338), the MINECO (Ministry of Economy and Competitiveness, RTC-2015-3693-1) and the Basque Government (IT1162-19) partially supported this study. The following institutions and projects supported authors' contracts: AM-B: Institute of Health Carlos III (ISCIII, PI16/02200), JG: University of the Basque Country (UPV/EHU); JB-E: *Govern Balear-Direcció General d'Innovació i Recerca* (predoctoral fellowship, FPI/1787/2015), DHL and RF: Ministry of Economy and Competitiveness (RTC-2015-3693-1) and GB-C: ISCIII (*Miguel Servet* II program, CPII17/0005). Further, contracts and projects were co-funded either by the European Regional Development Fund (ERDF) or the European Social Fund (ESF). Technical and human support provided by the *Plataforma de Microscopía* of IdISBa and by the *Servicio de Lipidómica* of the SGIKER (UPV/EHU, MICINN, GV/EJ, ESF) is gratefully acknowledged.

REFERENCES

1. Baker TC, Han J, Borchers CH (2017) Recent advancements in matrix-assisted laser desorption/ionization mass spectrometry imaging. Curr Opin Biotechnol 43:62–69 . doi: 10.1016/j.copbio.2016.09.003
2. Oetjen J, Lachmund D, Palmer A, Alexandrov T, Becker M, Boskamp T, Maass P (2016) An approach to optimize sample preparation for MALDI imaging MS of FFPE sections using fractional factorial design of experiments. Anal Bioanal Chem 408:6729–6740 . doi: 10.1007/s00216-016-9793-4
3. Swales JG, Dexter A, Hamm G, Nilsson A, Strittmatter N, Michopoulos F, Hardy C, Morentin-Gutierrez P, Mellor M, Andren PE, Clench MR, Bunch J, Critchlow SE, Goodwin RJA (2018) Quantitation of Endogenous Metabolites in Mouse Tumors Using Mass-Spectrometry Imaging. Anal Chem 90:6051–6058 . doi: 10.1021/acs.analchem.7b05239
4. Schwamborn K, Kriegsmann M, Weichert W (2017) MALDI imaging mass spectrometry — From bench to bedside. Biochim Biophys Acta - Proteins Proteomics 1865:776–783 . doi: 10.1016/j.bbapap.2016.10.014
5. Alexandrov T (2012) MALDI imaging mass spectrometry: statistical data analysis and current computational challenges. BMC Bioinformatics 13:S11 . doi: 10.1186/1471-2105-13-S16-S11
6. Jurchen JC, Rubakhin SS, Sweedler J V (2005) MALDI-MS imaging of features smaller than the size of the laser beam. J Am Soc Mass Spectrom 16:1654–1659 . doi: 10.1016/j.jasms.2005.06.006
7. Garate J, Fernández R, Lage S, Bestard-Escalas J, Lopez DH, Reigada R, Khorrami S, Ginard D, Reyes J, Amengual I, Barceló-Coblijn G, Fernández JA (2015) Imaging mass spectrometry increased resolution using 2-mercaptobenzothiazole and 2,5-diaminonaphtalene matrices: application to lipid distribution in human colon. Anal Bioanal Chem 407:4697–4708 . doi: 10.1007/s00216-015-8673-7
8. Lopez DH, Bestard-Escalas J, Garate J, Maimó-Barceló A, Fernández R, Reigada R, Khorrami S, Ginard D, Okazaki T, Fernández JA, Barceló-Coblijn G (2018) Tissue-selective alteration of ethanolamine plasmalogen metabolism in dedifferentiated colon mucosa. Biochim Biophys Acta - Mol Cell Biol Lipids 1863:928–938 . doi: 10.1016/j.bbalip.2018.04.017
9. Bestard-Escalas J, Garate J, Maimó-Barceló A, Fernández R, Lopez DH, Lage S, Reigada R, Khorrami S, Ginard D, Reyes J, Amengual I, Fernández JA, Barceló-Coblijn G (2016) Lipid fingerprint image accurately conveys human colon cell pathophysiologic state: A solid candidate as biomarker. Biochim Biophys Acta - Mol Cell Biol Lipids 1861:1942–1950 . doi: 10.1016/j.bbalip.2016.09.013
10. Sparvero LJ, Amoscato AA, Dixon CE, Long JB, Kochanek PM, Pitt BR, Bayır H, Kagan VE (2012) Mapping of phospholipids by MALDI imaging (MALDI-MSI): realities and expectations. Chem Phys Lipids 165:545–562 . doi: 10.1016/j.chemphyslip.2012.06.001
11. Dufresne M, Guneysu D, Patterson NH, Marcinkiewicz MM, Regina A, Demeule M, Chaurand P (2017) Multimodal detection of GM2 and GM3 lipid species in the brain of mucopolysaccharidosis type II mouse by serial imaging mass spectrometry and immunohistochemistry. Anal Bioanal Chem 409:1425–1433 . doi: 10.1007/s00216-016-0076-x
12. Duncan KD, Fang R, Yuan J, Chu RK, Dey SK, Burnum-Johnson KE, Lanekoff I (2018) Quantitative Mass Spectrometry Imaging of Prostaglandins as Silver Ion Adducts with Nanospray Desorption Electrospray Ionization. Anal Chem 90:7246–7252 . doi: 10.1021/acs.analchem.8b00350
13. Cahill JF, Kertesz V, Van Berkel GJ (2015) Characterization and Application of a Hybrid Optical Microscopy/Laser Ablation Liquid Vortex Capture/Electrospray Ionization System for Mass Spectrometry Imaging with Sub-micrometer Spatial Resolution. Anal Chem 87:11113–11121 . doi: 10.1021/acs.analchem.5b03293
14. Korte AR, Yandeau-Nelson MD, Nikolau BJ, Lee YJ i. (2015) Subcellular-level resolution MALDI-MS imaging of maize leaf metabolites by MALDI-linear ion trap-Orbitrap mass spectrometer. Anal Bioanal Chem 407:2301–2309 . doi: 10.1007/s00216-015-8460-5
15. Kertesz V, Van Berkel GJ (2008) Improved imaging resolution in desorption electrospray ionization mass spectrometry. Rapid Commun Mass

Spectrom 22:2639–2644 . doi: 10.1002/rcm.3662
16. Bokhart MT, Manni J, Garrard KP, Ekelöf M, Nazari M, Muddiman DC (2017) IR-MALDESI Mass Spectrometry Imaging at 50 Micron Spatial Resolution. J Am Soc Mass Spectrom. doi: 10.1007/s13361-017-1740-x
17. Wiegelmann M, Dreisewerd K, Soltwisch J (2016) Influence of the Laser Spot Size, Focal Beam Profile, and Tissue Type on the Lipid Signals Obtained by MALDI-MS Imaging in Oversampling Mode. J Am Soc Mass Spectrom 27:1952–1964 . doi: 10.1007/s13361-016-1477-y
18. Boggio KJ, Obasuyi E, Sugino K, Nelson SB, Agar NY, Agar JN (2011) Recent advances in single-cell MALDI mass spectrometry imaging and potential clinical impact. Expert Rev Proteomics 8:591–604 . doi: 10.1586/epr.11.53
19. Fernández R, Carriel V, Lage S, Garate J, Díez-García J, Ochoa B, Castro B, Alaminos M, Fernández JA (2016) Deciphering the Lipid Architecture of the Rat Sciatic Nerve Using Imaging Mass Spectrometry. ACS Chem Neurosci 7:624–632 . doi: 10.1021/acschemneuro.6b00010
20. Fernández R, González P, Lage S, Garate J, Maqueda A, Marcaida I, Maguregui M, Ochoa B, Rodríguez FJ, Fernández JA (2017) Influence of the Cation Adducts in the Analysis of Matrix-Assisted Laser Desorption Ionization Imaging Mass Spectrometry Data from Injury Models of Rat Spinal Cord. Anal Chem 89:8565–8573 . doi: 10.1021/acs.analchem.7b02650
21. Lagarrigue M, Becker M, Lavigne R, Deininger S-O, Walch A, Aubry F, Suckau D, Pineau C (2011) Revisiting Rat Spermatogenesis with MALDI Imaging at 20-µm Resolution. Mol Cell Proteomics 10:M110.005991 . doi: 10.1074/mcp.M110.005991
22. Fernández R, Lage S, Abad-García B, Barceló-Coblijn G, Terés S, López DH, Guardiola-Serrano F, Martín ML, Escribá P V., Fernández JA (2014) Analysis of the Lipidome of Xenografts Using MALDI-IMS and UHPLC-ESI-QTOF. J Am Soc Mass Spectrom 25:1237–1246 . doi: 10.1007/s13361-014-0882-3
23. Irvine RF (2003) Nuclear lipid signalling. Nat Rev Mol Cell Biol 4:349–361 . doi: 10.1038/nrm1100
24. Maté SM, Brenner RR, Ves-Losada A (2006) Endonuclear lipids in liver cellsThis paper is one of a selection of papers published in this Special Issue, entitled The Nucleus: A Cell Within A Cell. Can J Physiol Pharmacol 84:459–468 . doi: 10.1139/y05-097
25. Ohsaki Y, Kawai T, Yoshikawa Y, Cheng J, Jokitalo E, Fujimoto T (2016) PML isoform II plays a critical role in nuclear lipid droplet formation. J Cell Biol 212:29–38 . doi: 10.1083/jcb.201507122
26. Zhang L, Vertes A (2018) Single-Cell Mass Spectrometry Approaches to Explore Cellular Heterogeneity. Angew Chemie Int Ed 57:4466–4477 . doi: 10.1002/anie.201709719

Graphical Abstract